



# Experimental Characterization of Upper Trailing Edge Flaps for Transonic Buffet Control

Alessandro D’Aguanno<sup>1</sup> · Ferdinand F. J. Schrijer<sup>1</sup> · Bas W. van Oudheusden<sup>1</sup>

Received: 31 March 2022 / Accepted: 19 October 2022 / Published online: 29 October 2022  
© The Author(s) 2022

## Abstract

This experimental study investigates the possibility of controlling transonic buffet by means of a trailing edge flap with an upward deflection (referred to as “upper trailing edge flap”, or: UTEF). Different geometries (straight and serrated) and dimensions of UTEFs (with heights ranging between 1 and 2% of the chord) have been studied with respect to their impact on the buffet behavior. The effectiveness of the UTEFs has been investigated with schlieren and particle image velocimetry (PIV) in the transonic-supersonic wind tunnel of TU Delft at  $Ma=0.70$ ,  $\alpha=3.5^\circ$ . The schlieren results demonstrated the efficacy of the use of UTEFs for reducing the range of the buffet oscillations when the height of the UTEF was equal to at least 1.5%c. This result was corroborated by a flow characterization with PIV data and which highlighted that, in presence of a control system, not only the shock oscillation range is reduced but also the intensity of the separated area pulsation. The use of serrated UTEFs, despite having an effect on the local flow field, was found to be ineffective in alleviating buffet oscillations. The adoption of the best behaving UTEF configuration (straight 2%c UTEF) proved to only slightly alter the circulation value compared to the clean configuration, while it also proved to be effective in an off-buffet condition ( $Ma=0.74$  and  $\alpha=2.5^\circ$ ).

**Keywords** Transonic buffet · Control system · Upper trailing edge flap · PIV · Serrations

## 1 Introduction

Transonic buffet is a phenomenon which consists in the oscillation of a shock wave on the suction side of a wing and takes place at a certain range of Mach number ( $Ma$ ), angle of attack ( $\alpha$ ) and Reynolds number ( $Re$ ) values. Such shock oscillations could lead to vibrations of the structure, referred to as buffeting, that may eventually even cause mechanical failure because of fatigue, or impart dangerous oscillations of the aerodynamic characteristics of the vehicle. For those reasons the operational flight envelope of an airplane is restricted in practice. Therefore, to optimize the performance of civil aircraft,

---

✉ Alessandro D’Aguanno  
a.daguanno@tudelft.nl

<sup>1</sup> Aerodynamics Section, Delft University of Technology, Kluyverweg 2, 2629HS Delft, The Netherlands

studies regarding the understanding and possible control of transonic buffet are relevant and ongoing.

Following first studies on transonic buffet that have already been undertaken as early as 1952 (Hilton and Fowler 2692), the phenomenon has been widely studied in the past 30 years, yet the exact mechanism on which buffet is based has not been completely understood. A first attempt of globally characterizing transonic buffet was done by Lee (1990), where the shock buffet oscillation was described as being sustained by a feedback mechanism. According to this model, disturbances created at the shock foot are convected downstream in the trailing edge separated area. These disturbances have the form of vortical structures, and are referred to as downstream traveling waves (DTWs). Once the DTWs reach the trailing edge, pressure waves (referred to as upstream traveling waves, UTWs) are generated, in order to respect the Kutta condition, and travel upstream towards the shock wave. The shock oscillation is sustained by the interaction between the shock itself and the UTWs, which, depending on the phase, force the shock to move either upstream or downstream. Despite this model giving similar values to many experimental and numerical studies, it was not in perfect agreement with them (Jacquin et al. 2009; Garnier and Deck 2010). An improvement of the feedback model has been proposed by Deck (2005), where the UTWs are considered capable of traveling along the pressure side as well as the suction side. Hartmann et al. (2013) stated that the UTWs start reaching the shock in the last part of its downstream movement, thus forcing the shock to move upstream again. On the other hand, during the upstream movement, the area of separated flow widens, which reduces the formation of DTWs and consequently of UTWs, therefore, the shock upstream movement is not sustained by the UTWs anymore closing the feedback mechanism. The recent study of D'Aguanno et al. (2021a) experimentally confirmed the hypothesis of Hartmann et al. (2013), showing that the intensity of the UTWs is modulated during the buffet cycle. A further investigation of the DTWs dynamics was given in Feldhusen-Hoffmann et al. (2021), where, using dynamic mode decomposition, a vortex mode with the same frequency of the UTWs was captured.

Crouch et al. (2007) performed a stability analysis to determine the buffet onset, obtaining results which accurately predict the  $Ma$  and  $\alpha$  onset values, and are in good agreement with experimental data.

It is clear that to reduce the impact of transonic buffet, and thus increase the flight envelope, the use of a control system is beneficial. In the last two decades both active and passive control systems have been investigated as described in the review paper of Giannelis et al. (2017). As discussed in the following outline, buffet control systems are generally located either near the shock wave oscillation range or in the separated area or in the trailing edge area, with the goal of directly stabilizing the shock position or the separated area extent.

An example of an active control system for limiting transonic buffet is the use of a trailing edge deflector (TED), whose deflection is controlled in closed loop in response to the instantaneous position of the shock wave. This approach was taken in the study by Caruana et al. (2005), where the instantaneous value of the shock position is inferred from unsteady pressure measurements on the surface of the airfoil. The results showed the possibility of controlling transonic buffet by basically eliminating the shock oscillations. Similar TEDs have also been studied numerically by Gao et al. (2016); Ren et al. (2020), where respectively a linear delayed control law and an adaptive control strategy based on neural network (both with a feedback signal on the lift) have been employed, managing in both cases to stabilize the shock movement. The use of a closed loop control system is therefore very efficient in controlling transonic buffet, but requires quite a complex actuation system,

which could affect the reliability of the whole system. Thus, when simplicity and robustness is preferred, a passive control system may be more advantageous.

A simple passive control system is a vortex generator, which is a device that energizes the boundary layer helping the flow to remain attached longer and therefore to delay the oscillation of the separation area extent, which is a key element of transonic buffet. This kind of control system used by Caruana et al. (2003), demonstrated to be effective in reducing the amplitude of the buffet oscillation and in moving the buffet onset to higher values of the angle of attack, however, it decreases the lift/drag ratio when there is no separated flow. In recent years also fluidic vortex generators in the form of air jets located upstream of the shock location have been investigated (Brion et al. 2019). These devices can effectively reduce the extent of the separated area and postpone the buffet onset without increasing drag in cruise conditions (Molton et al. 2013). To avoid energy cost in the production of air jets, Brutyan et al. (2019) have proposed to actuate the jet (located in the supersonic area) with a passive air by-pass from the high pressure area downstream of the shock wave.

A particular form of vortex generator is the 3D shock control bump (SCB), which is characterized by geometry, consisting of a ramp, a crest, a tail and by angular side flanks. With this device the quasi-normal shock wave is replaced by a  $\lambda$ -shaped shock wave, with the working principle extensively described by Bruce and Colliss (2015). Colliss et al. (2016); Ogawa et al. (2008) have confirmed that an array of 3D SCBs is more efficient than a 2D bump configuration (which spans along the full span of the model as described in detail by Zhang et al. (2021)) in view of the streamwise vortices developing from the tail of the bumps. Applications of the use of SCBs for controlling buffet are discussed in the numerical studies of Mayer et al. (2018) and Geoghegan et al. (2020), which confirmed the dependence of the performance of a SCB on its size, shape and position relative to the shock. Similarly D'Aguanno et al. (2021b) experimentally showed the dependence of the control efficacy on the spanwise spacing of the SCBs. Therefore, the effectiveness of this device is not always guaranteed in conditions different from those for which the bump is designed (i.e. the fully developed buffet condition).

Trailing edge modifications can also be used as a passive control system, in the form of a flap with a fixed deflection. This typology of control system has been investigated by Despre et al. (2001), where a delay of the buffet onset was obtained for the lift coefficient, for different values of flap deflections. In particular, for the clean airfoil the buffet onset is obtained at  $C_L=0.97$ , while with a deflection of the TED of  $\delta=15^\circ$  at  $C_L=1.04$ .

A further example of a trailing edge modification is the use of a serrated trailing edge. However, although their effectiveness in reducing the emission of pressure waves having been confirmed for the low compressible flow regime, there is as yet no proof of their efficacy at transonic conditions (Nies and Olivier 2013).

In view of the described feedback mechanism of buffet, an alternative strategy of controlling buffet could be achieved by attempting to alter the communication between the separated trailing edge area and the trailing edge itself, which is responsible for the creation of UTWs. This motivates the implementation of a fixed flap with a vertical upward deflection at the trailing edge of the airfoil, also referred to as upper trailing edge flap (UTEF).

From a geometrical point of view, a UTEF resembles a Gurney flap (GF), which has been used both in automotive and aeronautic applications, respectively with an upward (for increasing downforce) and a downward flap deflection (Suresh and Sitaram 2011; Wanga et al. 2008) (for lift augmentation on a wing). Notwithstanding the geometrical similarity, the working principles of a UTEF and of a GF under buffet conditions are very different, with the former not expected to be associated with a modification of the lift coefficient when its height is small, since the UTEF is completely immersed in the trailing edge

separated area. An application of a UTEF for controlling transonic buffet is described in the numerical investigation by Tian et al. (2018), which showed the possibility of shifting the buffet onset to higher values of angle of incidence and lift coefficient. Different heights of UTEFs were studied, with the UTEF having a height of 1.5% of the chord of the airfoil giving the most promising results. Sartor et al. (2019) have also investigated the possibility of using a fluidic UTEF in the form of air jets operated at the trailing edge of the airfoil on the pressure side.

In the present study an experimental investigation on the use of upper trailing edge flaps for controlling transonic buffet will be performed using optical non-intrusive diagnostic techniques (schlieren and particle image velocimetry). In addition to straight UTEF configurations and a baseline configuration without flap, serrated UTEFs will be investigated as well. The latter may provide information on the effect of serrated trailing edge in compressible flows. To the best of the authors' knowledge no similar experimental study of this type has been previously reported in literature.

UTEFs may be considered as particular passive TEDs, however, they differ in several aspects. Regarding the use of passive TEDs in literature, Caruana et al. (2003) and Despre et al. (2001) considered only downward deflections ( $0^\circ < \delta < 50^\circ$ ), while in the study by Lee (1992), in view of the large chord of the flap ( $c_{\text{flap}} = 13\%c_{\text{airfoil}}$ ), only small deflection angles were considered. Thus, a UTEF is a specific TED geometry which has never been studied experimentally in literature for controlling transonic buffet. More importantly, the mechanism by which a UTEF is supposed to mitigate buffet is different from that of conventional TEDs, namely, not by directly affecting the circulation around the airfoil, but by interacting with the feedback loop referred to above. However, the stabilization of the buffet oscillations could indirectly affect the circulation, which should therefore be quantified. The use of a UTEF also differs very much from other passive control systems such as SCBs. These devices achieve a stabilization of the shockwave buffet oscillation by directly introducing the control system in the shockwave oscillation range, differently for the case of a UTEF no direct control of the shock position is attempted. Because of its expected working principle, the study of UTEF-based control configurations will also allow to achieve further insight into the physics of transonic buffet, particularly regarding the feedback mechanism occurring between the trailing edge of the airfoil and the oscillating shockwave. This aspect will be addressed by comparing the behavior of the different UTEF configurations (straight and serrated) with respect to the clean airfoil.

In the next section (Sect. 2) the experimental procedures are described. Subsequently (Sect. 3), a characterization of the shock dynamics is shown for all the tested configurations, using the schlieren visualization data. In Sect. 4 the differences between the most significant configurations are discussed, based on the particle image velocimetry (PIV) velocity field, also evaluating the aerodynamic effects induced by the presence of a UTEF. In Sect. 5 the sensitivity of the UTEF to the flow condition is discussed by analyzing the performance of a UTEF in a less developed buffet condition. In the conclusions (Sect. 6) the results are summarized and further discussed.

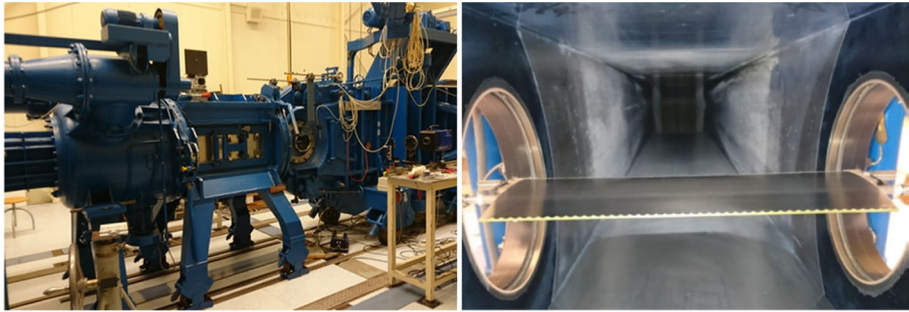


**Fig. 1** View of the TST-27 wind tunnel (left). Example of an upper trailing edge flap mounted on the OAT15A model in the test section (right)

**Table 1** Flow conditions

Parameter	Symbol	Value	Unit
Free stream Mach number	$Ma_\infty$	$0.7000 \pm 0.0005$	–
Total pressure	$p_0$	$2.000 \pm 0.005$	bar
Total temperature	$T_0$	$288.0 \pm 0.5$	K
Free stream velocity	$V_\infty$	$227.2 \pm 0.2$	m/s

## 2 Experimental Procedures

### 2.1 Wind Tunnel Facility

The experiments have been conducted in the transonic-supersonic blowdown wind tunnel of TU Delft, the TST-27 (see Fig. 1, left), which has a test section that is 255 mm high and 280 mm wide and has been fitted with solid walls for this investigation. This wind tunnel is able to establish transonic flow conditions with a variable choke located downstream of the test section. The accuracy of the Mach number is corrected to the third decimal digit by using a rotating wing in correspondence of the choke section. The experiments have been conducted for a free stream Mach number range  $Ma = 0.70 - 0.74$ , with a total pressure  $p_0 = 2 \text{ bars}$  and a total temperature  $T_0 = 288 \text{ K}$  as nominal stagnation conditions. The main experimental parameters are summarized in Table 1.

### 2.2 Model

The model used is the supercritical OAT15A airfoil (designed by ONERA (Jacquin et al. 2009)) with a span ( $b$ ) of 280 mm, a chord ( $c$ ) of 100 mm and a thickness to chord ratio  $t/c = 12.3\%c$  (see Table 2). A turbulent boundary layer has been ensured by placing a  $2\%c$  wide transition trip at 7% of the chord of the airfoil, made of Carborandum<sub>500</sub> particles (with a size of 0.014 mm). The airfoil has been mounted between the transparent side windows of the wind tunnel, allowing an optical access from both sides of the wind tunnel (Fig. 1, right). The windows can be rotated to vary the angle of incidence of the airfoil.

**Table 2** Model parameters

Parameter	Symbol	Value	Unit
Angle of attack	$\alpha$	$3.50 \pm 0.05$	
Chord	$c$	0.1	m
Span	$b$	0.28	m
Thickness to chord ratio	$t/c$	12.3	%
Reynolds number based on chord	$Re_c$	$(2.62 \pm 0.01) \cdot 10^6$	–

The model has been tested at  $Ma=0.70$  and  $\alpha=3.5^\circ$ , conditions for which buffet has been demonstrated to be fully developed (D'Aguanno et al. 2021c). The mentioned Mach number value differs from the value  $Ma=0.73$  obtained by Jacquin et al. (2009) for the most developed buffet condition for the same airfoil (also for  $\alpha=3.5^\circ$ ). However, it should be considered that the value reported in this study does not include wind tunnel corrections. Including a wind tunnel blockage correction, a corrected Mach Number of 0.73 is obtained (in good agreement with Jacquin et al. (2009)). This wind tunnel correction is computed with an empirical model based on the study of Herriot (1950). In addition, to assess the behavior of the UTEFs for less developed buffet conditions, tests with  $Ma=0.74$  and  $\alpha=2.5^\circ$  have also been carried out.

### 2.3 Upper Trailing Edge Flaps

The tested UTEFs have been realized as iron add-on profiles, with different heights and shapes (see Fig. 2, left). The three values of the height ( $h$ ) (with respect to  $c$ ) are:

- $h=1.0\%c$ ;
- $h=1.5\%c$ ;
- $h=2.0\%c$ .

These values have been chosen as to be in the order of the thickness of the boundary layer  $\delta$  at the trailing edge. It is worth mentioning that downstream of the shockwave, the boundary layer will become thicker, as shown by Babinsky and Harvey (2011). For this analysis a value of  $\delta=1.5$  mm is estimated from a turbulent boundary layer developing on

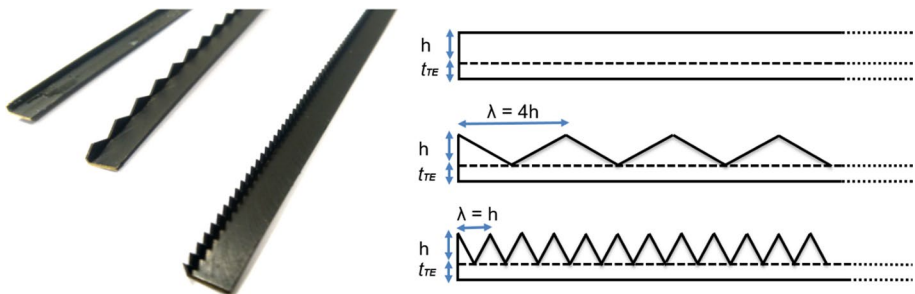


**Fig. 2** Shape of the upper trailing edge flaps, from the top to the bottom: straight, wide serration and narrow serration

an equivalent flat plate and is, thus, used only as a proxy of the real boundary layer thickness at the trailing edge.

The height ( $h$ ) is measured with respect to the suction side of the airfoil at the trailing edge (which for production reason has a thickness  $t_{TE}=0.75\%c$ ) and therefore, the real height of the flap (with respect to the pressure side) is given by the sum  $h+t_{TE}$  (see Fig. 2, right). For each value of  $h$ , three different shapes of UTEFs were tested:

- a straight UTEF;
- a wide serrated UTEF ( $\lambda/h=4$ );
- a narrow serrated UTEF ( $\lambda/h=1$ ).

where  $\lambda$  indicates the spanwise wavelength, i.e. the distance between consecutive teeth in the serration. A sketch of the different UTEFs is given in Fig. 2 while in Fig. 1 (right) the  $\lambda/h=4$ ,  $h=2\%c$  UTEF is visualized as mounted on the OAT15A airfoil.

## 2.4 Experimental Techniques

High speed schlieren and particle image velocimetry (PIV) have been used in order to investigate the effectiveness of UTEFs in limiting transonic buffet. The schlieren data is used to visualize and quantify the shock movement for the different UTEFs studied. A conventional z-configuration has been adopted, using a pinhole diameter of 2 mm. The field of view includes the full chord of the airfoil and the relative images have been acquired with a high speed camera Imager Pro 4MP. The camera has been operated with a cropped resolution of  $912\times 816$  pixels (7.6 pix/mm) with a frequency of acquisition of 5 kHz for a total time duration of 2 s (10,000 images) with an exposure time of 15  $\mu$ s. Considering that the expected buffet frequency is 160 Hz (D'Aguanno et al. 2021c), the selected acquisition frequency is high enough to resolve the shock position in time, obtaining nearly 30 images per buffet cycle.

In order to quantify the velocity field, a high speed PIV campaign has been performed, with a sketch of the set-up shown in Fig. 3 (right). Two Photron Fastcam SA-1 in 2C mode have been used, with the cameras placed on opposite sides of the wind tunnel to enlarge the overall field of view. The cameras acquire images at a frequency of 4.65 kHz in double pulse mode ( $\Delta t=3\ \mu$ s) with a resolution of  $1024\times 640$  pixels. As sketched in Fig. 3 (left), two partially overlapping field of views (FOVs) are present, both with a size of  $50\times 30\%c$  ( $50\times 30$  mm).  $FOV_1$  starts at  $26\%c$  from the leading edge, while  $FOV_2$  starts at  $72\%c$  (till

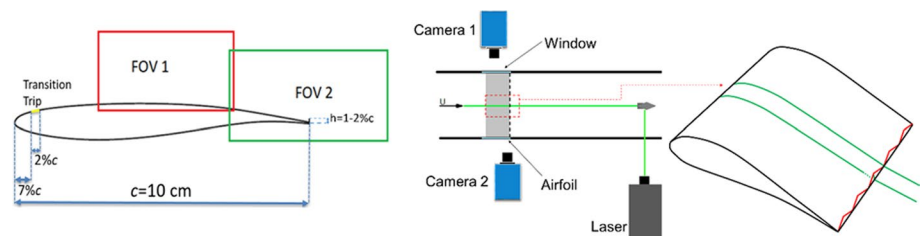


**Fig. 3** OAT15A airfoil with indication of the PIV FOVs (left). Sketch of PIV set-up, with detail for the two measurement planes used for the wide serrated UTEFs (right)



122%*c*) and therefore it includes part of the wake of the airfoil. Both cameras are equipped with a 105 mm focal length lens and an f-stop of 5.6.

To understand the behavior of the serrated UTEFs (for the wide serrated configurations) the PIV measurements have been conducted with the laser aligned either with the peak or the valley of the serration, in both cases in proximity of the mid span of the airfoil (see details in Fig. 3 (right)). A dual cavity high speed laser MESA PIV (Nd:YAG) has been used to illuminate the seeding particles in a 1.5 mm thick sheet. The tracer particles are DEHS (Di-Ethyl-Hexyl-Sebacat) particles, which have a relatively low relaxation time ( $\tau_p = 2 \mu\text{s}$ ) and are characterized in detail by Ragni et al. (Ragni et al. 2011). For the PIV acquisition the Davis software has been used (Version 8.4.0). In order to have a synchronization between the cameras and the laser, a LaVision High Speed Controller (art. 1108075) has been employed.

## 2.5 Data Processing

After the acquisition of the raw PIV snapshots, a pre-processing procedure has been used to reduce the effect of laser light reflections on the airfoil, which are particularly present at the trailing edge in presence of an UTEF. For this purpose a sliding time-minimum subtraction has been applied to the data sets, with the minimum evaluated for a kernel size of 11 images. For the cross-correlation, required to compute the velocity fields, a multi-pass approach has been applied with two passes with a window size of  $64 \times 64$  pixels and two passes with a final circular window size of  $24 \times 24$  pixels ( $1.2 \times 1.2$  mm). An overlap of 75% of the window size has been chosen resulting in a final vector spacing of 0.3% of the chord (0.3 mm).

For both schlieren and PIV data, additional processing was carried out in *Matlab*. A validation of the PIV instantaneous velocity fields included detection and correction of vector outliers, with the operation completed in two steps. In the first step the outliers are localized using the 3 standard deviation rule and replaced with an interpolation of the neighboring vectors (Westerweel and Scarano 2005). An additional interpolation in time has been completed to correct images with large group of outliers (for example due to the lack of seeding).

## 2.6 Uncertainty Analysis

A quantification of the uncertainty of the collected data is of utmost importance when it comes to a comparative analysis among different configurations, like in this study. In Table 3 the main sources of uncertainty are shown.

The strongest effect is the uncertainty associated with the particle slip and it is governed by the value of the relaxation time ( $\tau_p$ ) of the seeding particles (Ragni et al. 2011). The

**Table 3** Uncertainty errors

Uncertainty source	Error	Unit
Cross-correlation ( $\epsilon_{cc}$ )	$\leq 6.7$	m/s
Spatial resolution ( $\epsilon_{sr}$ )	$\leq 1$	%
Particle slip ( $\epsilon_{slip}$ )	$\leq 60$	m/s
Line of sight effect ( $\epsilon_{schlieren}$ )	0.003	m



uncertainty value reported in Table 3 ( $\epsilon_{slip} \leq 60$  m/s) is computed for the shock oscillation region, where the highest velocity gradients and therefore the highest particle slip effects are experienced. In the region without shock, this uncertainty contribution is of the same order of magnitude as the other uncertainties. The cross-correlation uncertainty is associated with the computation of the velocity fields from the raw images and is always lower than  $\epsilon_{cc} = 5$  m/s (Humble 2009). Furthermore, the choice of the window size limits the size of the smallest resolvable flow structure, which gives an additional uncertainty in the velocity field. For a multi-step correlation and considering that the smallest resolvable flow structure has twice the size of the window size, an error  $\epsilon_{sr}$  ( $u/u_0$ )  $< 1\%$  is present (see for more details (Schrijer and Scarano 2008; Kat and Oudheusden 2012)).

For the schlieren images the uncertainty is mainly connected with the error in the detection of the shock wave (SW) position. In these snapshots, all the density effects present along the line of sight are integrated, resulting in the shock wave appearing with a non-negligible width. The uncertainty due to the line of sight takes into account this effect and is estimated as half of the maximum width of the projected visualization of the shock wave.

### 3 Shock Dynamics

In this section the unsteady behavior of the shock wave is scrutinized for the different configurations by means of schlieren visualizations. First, the instantaneous images belonging to a typical buffet cycle are discussed for the airfoil equipped with a straight UTEF with a height of  $2\%c$  (see Fig. 4). The cycle is visualized showing representative snapshots for four relevant buffet phases: with the shock wave in its most upstream position; during the downstream travel; in the most downstream position and during the upstream travel. Considering the more extensive phase definition shown in the sketch in Fig. 5, these schlieren images correspond respectively to phases 1, 3, 5 and 7.

The selected FOV offers a complete view of the suction side of the airfoil (see Fig. 4). The presence of the transition trip located at  $7\%c$  results in the presence of an oblique pressure wave close to the leading edge in all the images. Notwithstanding the relatively

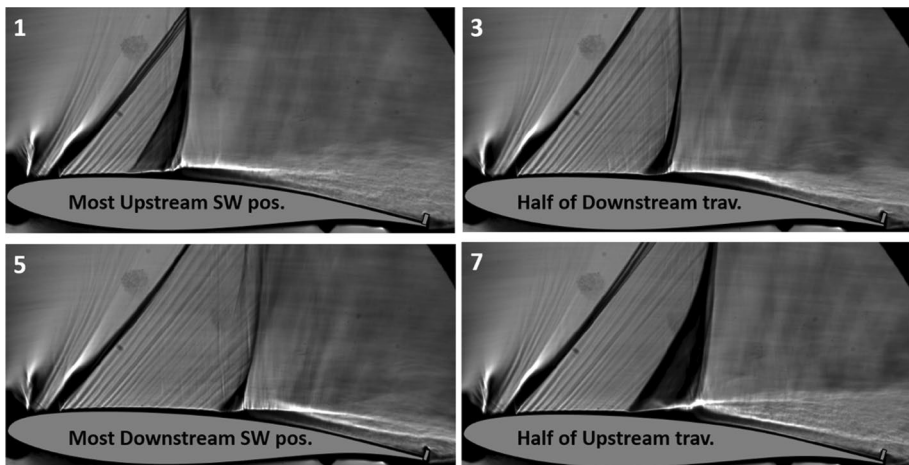
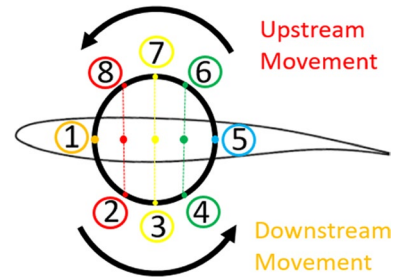


Fig. 4 Instantaneous schlieren images in four main phases for straight  $2\%$  UTEF configuration

Fig. 5 Buffet phase definition



prominent appearance of this wave in the visualization, the flow can be considered isentropic up to the location of the main shock wave that terminates the supersonic region.

In the first image on the top left of Fig. 4, the shock wave is in its most upstream position. In this phase the shock is visualized by a wide black line (in particular close to the surface of the airfoil) and it is located at around  $30\%c$ . The width of the shock wave line is connected to the presence of 3D effects along the span (developing, in particular, close to the side windows of the wind tunnel) and to the presence of a  $\lambda$ -shaped shock wave close to the surface of the airfoil. Due to the horizontal orientation of the schlieren knife edge, the downstream developing separated area over the airfoil is visualized as well. In the following phase (sub-figure on the top right) the shock wave is moving downstream (with the shock wave located at  $x \approx 40\%c$ ) and the separated area is reduced. As a result of this, the black line indicating the shock wave appears thinner and more normal with respect to the surface of the airfoil than in the previous image. In the visualization on the bottom left (phase 5) the shock wave reaches its most downstream location at  $x \approx 55\%c$ , with the separated area almost completely reattached. When the shock wave starts its upstream travel again (sub-figure on the bottom right), it acquires the highest velocity with respect to the flow, triggering a strong separation and a change in inclination of the shock wave.

For this discussion the straight  $2\%c$  configuration was used but for the clean airfoil and the airfoil with the other UTEFs a similar general behavior is observed. Nevertheless, some recurrent differences between some of the tested configurations have been observed as shown in Fig. 6. Starting from the sub-figures on the left, when a UTEF is used an upwash appears at the trailing edge of the airfoil, this feature is particularly evident when

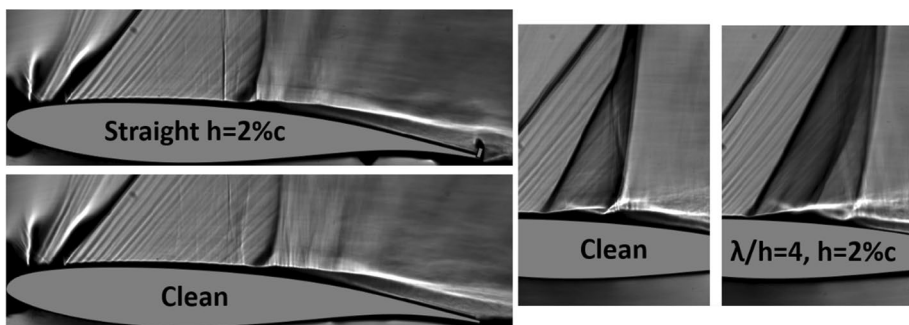


**Fig. 6** Difference in flow structures at the trailing edge, for the clean and straight UTEF configurations (left). Shock wave structures for clean and serrated UTEF ( $\lambda/h=4$ ,  $h=2\%c$ ) configurations during upstream movement (right)

the separated area reattaches during the last part of the downstream travel. Differently, during the upstream travel, additional 3D contributions to the shock wave visualization appear in presence of a serrated UTEF as visualized on the right of Fig. 6.

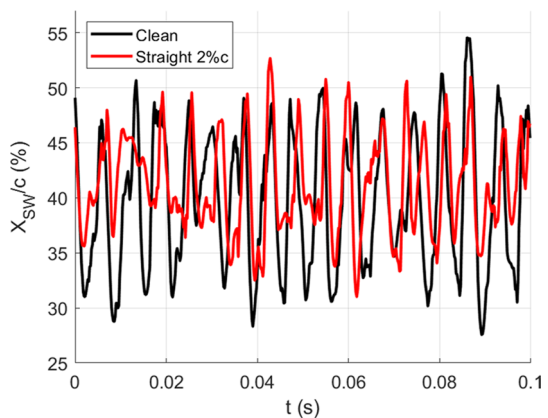
This observation suggests that the subsequent peaks and valleys of the teeth of the serration cause differences in terms of shock wave position and separated area along the span. Which is expected due to the upstream traveling waves which have a different strength in the peak or valley of the serration. This evidence supports the idea that the presence of UTEFs has a significant effect on the whole buffet mechanism and consequently on the shock position. The effect of the serration will be discussed in more details in Sect. 4.3.

### 3.1 Shock Position

From the schlieren images the shock position has been tracked in time by looking at the gradient of luminosity in each image. In order to reduce the errors associated with the shock detection, the shock wave position has been tracked along multiple horizontal lines at a vertical distance from the airfoil surface of 1 cm and the results are averaged. In Fig. 7 an example of the behavior of the shock position is shown for the clean and for the straight 2%*c* UTEF configurations. The plot shows that, in the selected time interval, the shock oscillation amplitude is reduced (of nearly 20%) for the UTEF case with the average shock position moved to slightly higher values (2–3%*c* more downstream). Furthermore, it seems that for the 2%*c* UTEF case, the shock position behavior is less periodic.

To quantitatively compare the range of oscillation of the shock wave, its distribution has been plotted (Fig. 8, left) in terms of probability density function (pdf) for different configurations (clean, straight  $h=1\%c$ , straight  $h=2\%c$  and serrated  $\lambda/h=4$  with  $h=2\%c$ ) using a bin size of 1%*c*. A reduced range of the shock wave position is obtained for the straight 2%*c* UTEF compared to the clean configuration. As a consequence, there is a narrower distribution of the pdf ( $p(X_{SW}/c)$ ), in comparison to the clean configuration where the most probable shock locations are spread over a wider range of chordwise positions. For the straight 2%*c* configuration, as seen in Fig. 7, the shock wave behavior is less periodic including significant amplitude variations, suggesting that the coherence of the buffet mechanism is somehow decreased. To substantiate the latter consideration, the oscillation amplitude of each buffet cycle ( $\Delta_{SW}$ , considered as the chordwise distance between consecutive locations in which the shockwave inverts its direction) has been computed and its

**Fig. 7** Comparison of the time behaviors of the shock position for clean and straight 2% configurations



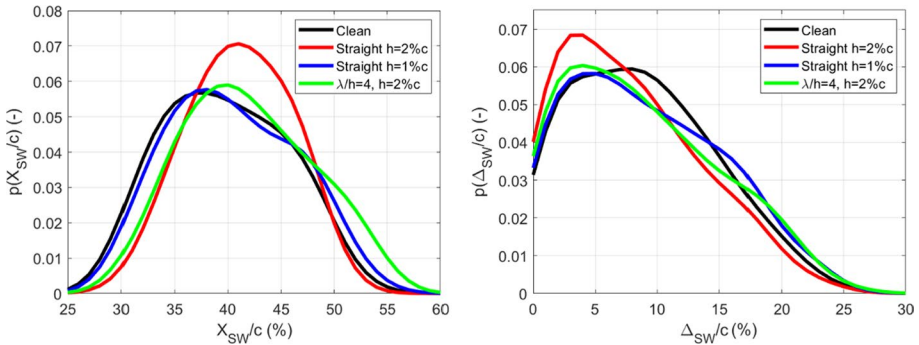


**Fig. 8** Comparison of the distribution of the shock position (left) and of the amplitude of shock wave oscillation (right) for different configurations

distribution  $p(\Delta_{SW}/c)$  is visualized in Fig. 8 (right). In the case of the clean airfoil, the most frequent amplitude of oscillation is in the order of  $10\%c$ , which is significantly higher than for the straight  $h=2\%c$  UTEF. For the latter case, cycles with an amplitude of oscillation lower than  $5\%c$  are very common.

In presence of a straight  $1\%c$  UTEF the range of oscillation of the shock wave is very similar to that of the clean airfoil, suggesting that this height of the UTEF is not sufficient for yielding a relevant impact on the transonic buffet mechanism. This confirms the necessity of having a height of the UTEF larger than the boundary layer thickness  $h \geq \delta(x=100\%c)$ . For the  $\lambda/h=4$ ,  $h=2\%c$  serrated UTEF, the amplitude of the shock wave oscillations is very similar to the clean case, but with a distribution ( $p(X_{SW}/c)$ ) that is moved to more downstream positions. Despite the different ranges, for all considered configurations the average shock position is between  $40$  and  $45\%c$ .

### 3.2 Spectral Analysis

The spectral content of the shock location in time is investigated by looking at the power spectral density (PSD). The Welch method (Welch 1967) has been used to reduce the noise, obtaining a maximum detectable frequency of  $2500$  Hz (half of the acquisition frequency) and a frequency resolution of  $4.9$  Hz.

In Fig. 9 (left) the PSD of the shock position ( $P$ ) is shown in its pre-multiplied form ( $f \cdot P$ ). To ease the visualization of the data, only the results for the clean and the straight  $2\%c$  configuration have been plotted, with both PSDs normalized by the variance of the shock oscillation signal for the clean case. Both configurations have a main peak at a frequency of  $160$  Hz, which corresponds to a Strouhal number  $St = U_\infty \cdot f/c = 0.07$ , which is in perfect agreement with the results obtained by Jacquin et al. (2009). Secondary peaks arise at  $320$  Hz (second harmonic of buffet) and at  $410$  Hz, which is a contribution associated to the characteristic noise of the wind tunnel. The result shows that the application of the UTEF does not have an effect on the value of the main frequency contribution ( $160$  Hz) but reduces the amplitude of this frequency peak by nearly  $60\%$  compared to the clean airfoil, without any apparent increase of energy for the secondary peaks. This observation confirms that, by using UTEFs, the feedback mechanism is not completely eliminated, but attenuated.

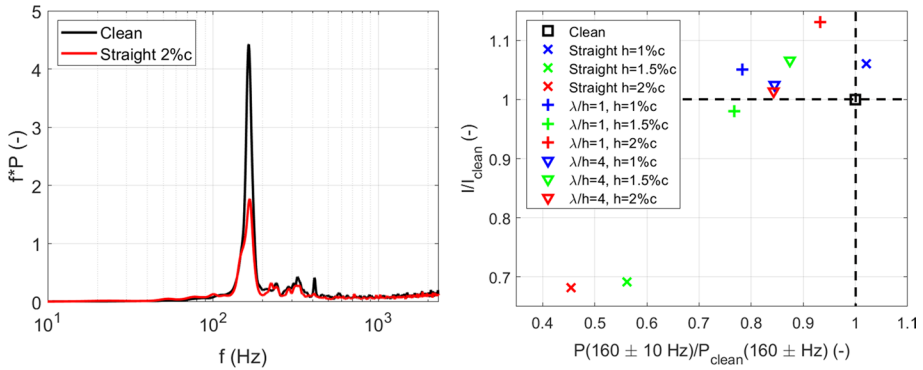


**Fig. 9** Comparison of PSD for clean and straight 2% configurations (left) and integral value of PSD for all the configurations studied (right)

To quantitatively verify whether, with the use of a UTEF, the energy associated with the shock oscillation is just reduced overall or distributed to secondary frequency contributions, the PSD is integrated in the frequency range  $f=0\text{--}1000$  Hz, excluding high frequency contributions. These contributions are typically associated with erroneous shock-wave detections caused by the inherent uncertainty in tracking the shockwave position due to the spanwise integration of the density gradients. The corresponding integral value ( $I$ ) is plotted in Fig. 9 (right) against the value of  $f \cdot P$  at  $160 \pm 10$  Hz (main peak). Both values are normalized by the values of  $I$  and  $f \cdot P$  for the clean airfoil. By definition the value for the clean configuration is 1 for both the abscissa and the ordinate. It is evident that the UTEFs which behave best in reducing the buffet intensity are the straight configurations with heights of 1.5% and 2% of the chord, for which a reduction of integral energy of respectively 31 and 32% and of the main peak of 45 and 55% is observed (compared to the clean airfoil). Therefore, for  $h \geq 1.5\%c$  a very similar performance of the UTEFs is obtained, however, to have a more precise optimization of the choice of the height of the UTEF further tests should be carried out on UTEFs with larger values of  $h$ . The results for  $h \geq 1.5\%c$  differ very much from the performance of a straight UTEF with a height of only 1%*c*, for which a behavior similar to the clean configuration is present. This observation confirms that the height of 1%*c* is insufficient to affect the structures developing below the separated shear layer and boundary layer and suggests that the thickness of this layer is well approximated by the estimation given in Sect. 2.3.

The use of the serrated UTEFs leads to either a negligible reduction of the relevance of buffet or even a small increase, confirming the inefficacy of serrations in compressible applications.

## 4 Velocity Field Comparison

### 4.1 Flow Field Statistics

The straight UTEF with a height of 2%*c* was one of the two best performing configurations (together with the 1.5%*c* straight UTEF) and is analyzed more in detail in this section, in

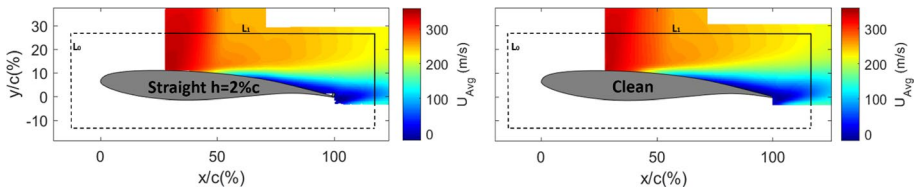


**Fig. 10** Time-average horizontal velocity component for straight 2% and clean configuration. The solid black line indicates the line ( $L_1$ ) on which the contribution to the circulation in the FOV is computed, while on the dashed line ( $L_0$ ) outside the FOV, the flow conditions are assumed to be independent from the trailing edge configuration

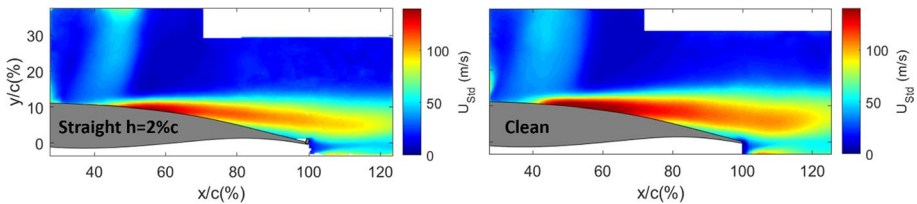


**Fig. 11** Standard deviation of the horizontal velocity component for straight 2% and clean configuration

comparison to the clean configuration. The effect of serrated UTEFs will then be addressed in Sect. 4.3.

Figure 10 provides a comparison of the time-average horizontal component of the velocity field for the two configurations of primary interest. With respect to the clean configuration (right), a small reduction of the separated area is observed in presence of the straight UTEF (left). To better appreciate the differences in flow unsteadiness between the two configurations, the standard deviation of the horizontal velocity component ( $u_{STD}$ ) is shown in Fig. 11. Main differences are visible in both the shock wave oscillation area and in the separated region. It is evident that with the use of a UTEF there is a relevant reduction of the shock wave oscillation range (reducing from 20% $c$  for the clean case to around 10% $c$  for the UTEF configuration).

A similar reduction is present for the fluctuations in the separated area, as shown by the vertical extent of the region in which the values of  $u_{STD}$  are larger than 80 m/s, which drops from 6.6 to 4.2% $c$  for the UTEF configuration. This comparison confirms that with the UTEF the unsteadiness in the flow field is substantially reduced.

In order to appreciate how these variations are reflected in the different buffet stages, a phase average of the velocity field is computed by means of a triple decomposition, according to:

$$u = u_{avg} + u_{per} + u_{rand} \quad (1)$$

Thus, the velocity field is described as the sum of a mean ( $u_{avg}$ ), a periodic ( $u_{per}$ ) and a quasi-random fluctuating ( $u_{rand}$ ) term. According to the sketch in Fig. 5 the PIV images have been divided in eight different bins (phases) according to shock wave position and to its direction of movement. Subsequently, an average velocity field has been computed for each phase.

In Fig. 12 the phase averaged horizontal velocity field (given by the sum of the mean and the periodic contributions,  $u_{phs} = u_{avg} + u_{per}$ ) is shown for the clean and UTEF



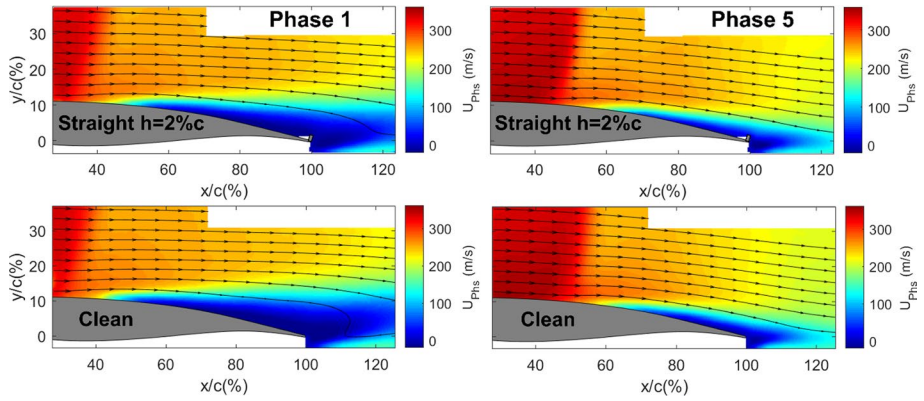
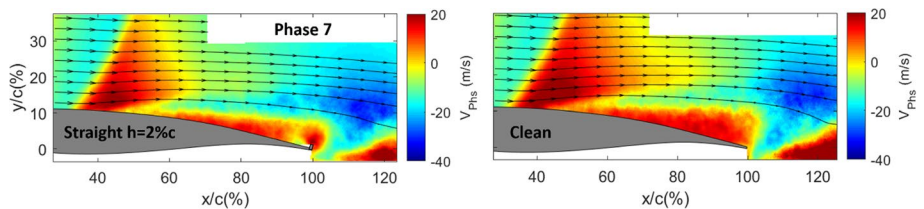


**Fig. 12** Comparison of horizontal phase-averaged velocity field in phases 1 (left) and 5 (right) for straight 2% (top) and clean configuration (bottom)

configurations in the phases in which the shock wave is either in the most upstream (phase 1) or in the most downstream position (phase 5). For a more detailed analysis of the phase averaged velocity field for the clean airfoil, the reader is referred to D’Aguanno et al. 2021c.

From a first comparison of the velocity fields, the UTEF appears to reduce the oscillation range of the shock wave (in agreement with the results shown in Sect. 3.1). In more detail, in phase 1 the shock wave is located more upstream and the separated area is wider for the clean configuration, as is also observable from the direction of the streamlines close to the surface of the airfoil. In phase 5 the shock wave has reached its most downstream position and it is located more upstream for the UTEF configuration. No important difference is instead observable for the extent of the separated area size (the flow is almost completely reattached in this phase) or for the direction of the streamlines.

Another significant phase of transonic buffet is phase 7, in which the shock wave is halfway during its upstream travel. At this stage the shock wave has the highest relative velocity with respect to the flow. Therefore, this is the phase in which the extent of the separated area is at its maximum and as a consequence the shock wave is more oblique. This phase is best characterized by the behavior of the vertical component of the velocity field, as shown in Fig. 13. A wide area of positive vertical velocity occurs at the shock foot because of the presence of the oblique shock wave as well as a wide separated trailing edge area extending from the the trailing edge up to the shock. These features occur for both the configurations, but with important differences being observable just upstream of the UTEF.

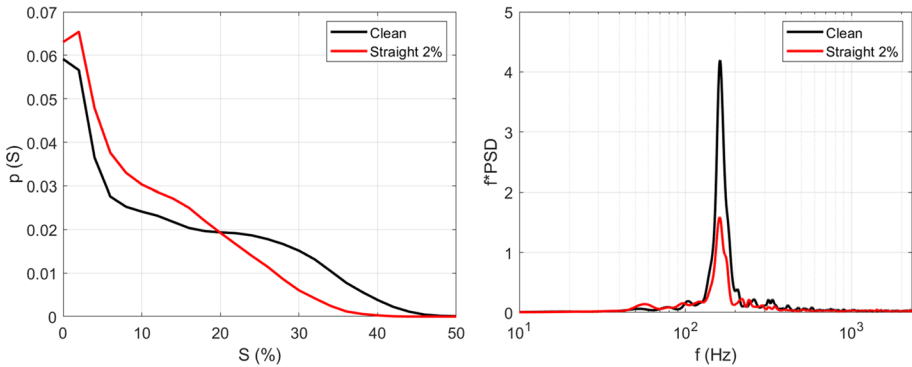


**Fig. 13** Comparison of vertical phase-averaged velocity field in the 7th phase for straight 2% and clean configuration



**Table 4** Separated area extent statistics

Configuration	$S_{avg}$ (%)	$S_{std}$ (%)
Clean	13	12
Straight 2% UTEF	9	9
Serrated, wide UTEF 2% valley	18	12
Serrated, wide UTEF 2% peak	16	12

**Fig. 14** Comparison of distribution of separated area size (left). Spectral analysis of separated area extent (right)

The extent of both these regions is reduced in presence of a UTEF suggesting that accordingly the strength of the shock wave is reduced as well. This behavior may be attributed to the lower velocity of the shock wave in presence of the straight 2% UTEF, since the shock wave oscillation range is reduced but the buffet frequency remains constant. The reduction of the separated area has also been associated with the presence of a clockwise vortex at the back of the flap and upwash behind the airfoil, as shown by Tian et al. (2018) in their numerical investigation.

## 4.2 Separated Area Extent

Together with the shock position behavior, which has been analyzed in detail in Sect. 3.1, another key element of transonic buffet is the pulsation of the separated area size. The extent of the separated area has been computed for each instantaneous PIV image, by determining the percentage of vectors ( $S$ ) with a velocity lower than 0 m/s in a rectangular region which ranges from 60 to 100% $c$  and for a height of 25% $c$  over the surface of the airfoil. The average extent of the separated and its standard deviation value are reported in Table 4, confirming a reduction of more than 25% of both the average extent ( $S_{avg}$ ) and the pulsation (indicated by its standard deviation,  $S_{std}$ ) of the separated area size in presence of the straight 2% UTEF.

The distribution of the separated area extent for the two studied configurations is plotted in Fig. 14 (left). For both the clean and the UTEF configuration the higher values of the distribution are obtained for  $0\% < S < 4\%$ , which corresponds to a very limited (but not zero) separated area. This peak confirms that, usually, when the shock foot

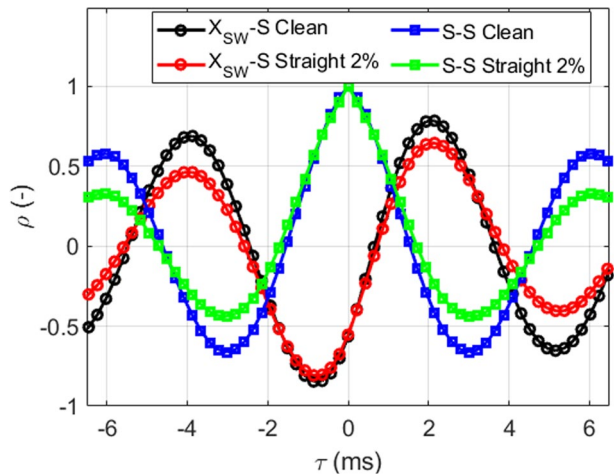
separation is absent, there is still a small area in the FOV (for both the configurations), in which an area persists where the velocity is smaller than 0 m/s.

This corresponds to the trailing edge separated area and is also visible in Fig. 12 (right). For the clean configuration, values of  $S$  between 10 and 30% are similarly probable, indicating that, along the buffet cycle, the separated area is expanding and shrinking in a wide range. Differently, for the straight UTEF configuration very few snapshots have values of  $S$  higher than 25% ( $p(S) < 0.01$ ). This distribution suggests that in the majority of the buffet cycles the separated area remains relatively small compared to the clean configuration.

Knowing the extent of the separated area in each time step, the relative spectral content has been determined, as plotted in Fig. 14 (right) in the form of a pre-multiplied PSD. Both the configurations have a main contribution at 160 Hz, but the value is reduced by more than 50% in presence of the straight 2% UTEF; in good agreement with the spectral analysis of the shock position (again in terms of amplitude, see Fig. 9 left).

To further characterize the temporal behavior of the separated area, the autocorrelation of the separated area signal ( $S$ ) is plotted in Fig. 15. For a time separation equal to one complete buffet cycle period ( $\tau = 6.2$  ms), the autocorrelation value is 0.32 for the UTEF case (green line), while 0.58 for the clean configuration (blue line). This indicates that in presence of UTEF the oscillations of the separated area are not only of lower amplitude but also more irregular (i.e., less coherent), with the extent of the separated area varying significantly in different buffet cycles (as already pointed out for the shock position in Fig. 8, right). To check whether the relationship between the separated area extent and the shock wave position is influenced by the presence of the straight 2% UTEF, the cross-correlation between these two quantities is shown in Fig. 15 as well. The correspondence between the two results (all the positive and negative peaks of the cross-correlation occur for the same values of  $\tau$ ) confirms that the physics of the phenomenon has not changed substantially. However, once again the correlation drops off with time separation more rapidly for the UTEF case, similar as for the shock-position autocorrelation. The main peak (in terms of absolute value) is obtained for  $\tau = -0.65$  ms. This indicates that the widest separated area is obtained shortly before

**Fig. 15** Autocorrelation in time of separated area extent and cross-correlation in time between shock wave position and separated area extent



the most upstream shock position is reached. However, it is evident that the values of the different minimums and maximums of the cross-correlation are smaller in presence of UTEFs (red line). Hence, the dependence between shock wave and separated area is less defined in presence of UTEF than for the clean airfoil (black line).

### 4.3 Effect of Serrated UTEF

As already observed in the schlieren images, strong 3D effects arise when mounting a serrated UTEF. To better understand these effects, the PIV results are analyzed for the  $\lambda/h=4$ ,  $h=2\%c$  serrated-UTEF configuration and compared to the straight  $2\%c$  and the clean configuration. For the serrated case the velocity field data is shown for two spanwise locations, the peak and the valley of the serration (see Fig. 3, right).

In Fig. 16 a comparison is shown of the average vertical velocity field for the previously mentioned configurations. Since no important difference was present for the horizontal component of velocity, these results are omitted. For the vertical velocity field corresponding to the peak of the serration (Fig. 16, bottom-left), a small reduction of velocity at the trailing edge is observed with respect to the data collected in the plane corresponding to the valley of the serration (Fig. 16, bottom-right).

This difference is particularly evident in proximity of the serration ( $95\% \leq x/c \leq 100\%$ ), where upwash is present. This evidence is in good agreement with the comparison between the straight  $h=2\%c$  and the clean configuration, confirming the effect of the UTEF on the flow near the trailing edge. A reduction in the extent of the separated area is obtained for the straight UTEF compared to the clean configuration. For both the serrated configurations an increase of the separated area extent is observed with respect to both the clean and the straight  $2\%c$  configurations. However for the serrated  $\lambda/h=4$ ,  $h=2\%c$  UTEF a reduction of the separated area is obtained in the plane corresponding to the peak with respect to the plane corresponding to the valley. These qualitative observations are quantified by the data shown in Table 4 where the average values of  $S$  have been given for the different configurations. In particular, for the serrated configurations, the occurrence of shock-foot separated area appears to be less intermittent, with the separated area apparently extending from the shock foot till the trailing edge also in the mean flow field. When looking at

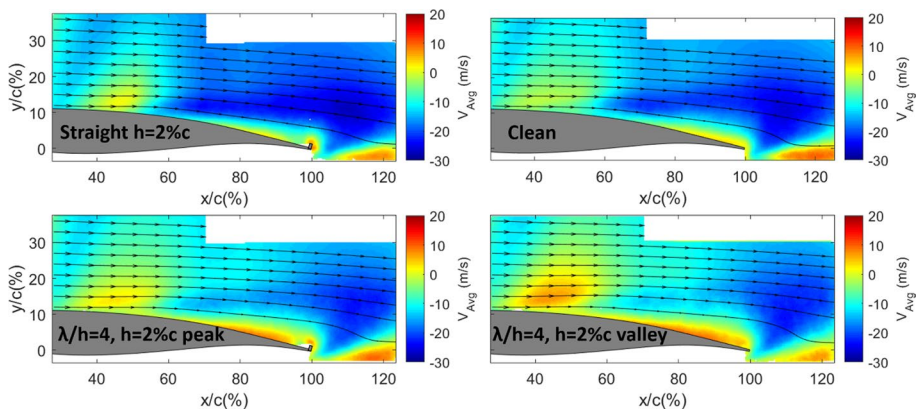


**Fig. 16** Comparison of the vertical averaged velocity field for clean airfoil, straight  $h=2\%$  UTEF and  $\lambda/h=4$ ,  $h=2\%$  UTEF in the peak and in the valley of serration

the standard deviation of  $S$ , comparable values for the two planes of the  $\lambda/h=4$ ,  $h=2\%c$  serrated-UTEF configuration (peak and valley of serration) are obtained, with significantly lower values achieved for the straight UTEF configuration. Thus, although there is an increase in the average extent of the separated area for the serrated configurations, the corresponding fluctuations are unchanged with respect to the clean configuration, in agreement with the unsteadiness of the shockwave position (see Fig. 9, right).

Comparing the average velocity fields in Fig. 16, additional differences are present in the shock oscillation area, with a larger increase of the vertical velocity in the measurement plane corresponding to the valley of the serration (as compared to the peak location). As previously commented, in this measurement plane the separated area is on average wider than for the measurement plane aligned with the peak, and therefore, the shock wave is more inclined (oblique), resulting in a higher increase of vertical velocity at the shock foot.

The results discussed in this subsection show that in presence of a serrated UTEF, the flow behaves differently according to the span location of the measurement plane. In particular, in the plane passing at the peak of the serration, the flow field is locally more similar to the flow field for the straight UTEF configuration, while in the valley it is more similar to the clean configuration. No strong difference is obtained in terms of the unsteadiness (shock oscillation and separated area pulsation). This suggests that the local presence of the peak or of the valley of the serration is influencing the flow distribution in the vicinity of the UTEF, but does not affect the overall buffet mechanism.

#### 4.4 Circulation Evaluation

From the previous sections it is clear that the use of a straight UTEF has a positive effect by reducing both the shockwave oscillations and the separated area pulsations associated with fully developed transonic buffet. Nevertheless, it could be conceived that the application of a UTEF might induce a reduction in lift and by that could move the most developed buffet conditions to higher values of  $Ma$ ,  $\alpha$ . In order to investigate this possible effect, the PIV data have been further processed to get an estimation of the change in circulation ( $\Gamma$ ) when introducing the UTEF. This has been done first for the average and later for the phase averaged velocity fields. The circulation around the airfoil can be described as:

$$\Gamma = \Gamma_0 + \Gamma_1 \quad (2)$$

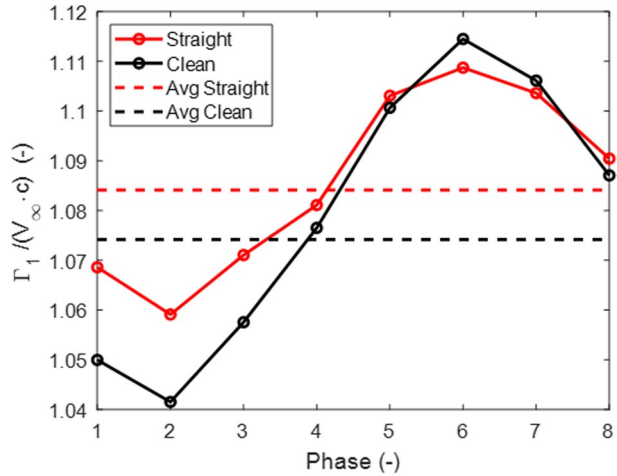
With  $\Gamma_1$  being the contribution of the circulation computed in the PIV FOV (along the partial contour  $L_1$  as indicated in Fig. 10) and  $\Gamma_0$  the contribution on the remaining sector ( $L_0$ ). In this analysis only the term  $\Gamma_1$  is evaluated explicitly, while it is tentatively assumed that the value of  $\Gamma_0$  is similar for the different configurations. This assumption is associated with the fact that no difference in the velocity field is expected to be present in the supersonic area upstream of the selected FOV (since disturbances cannot travel back from the subsonic trailing edge area to the supersonic area) or along the pressure side (in view of the upward vertical deflection of the trailing edge flap). In addition, in the approximation of a potential flow it can be derived that a change in the partial circulation  $\Gamma_1$  is proportional to a change in the total circulation  $\Gamma$  ( $d\Gamma_1 = c_1 \cdot d\Gamma$ , where  $c_1$  is a constant depending on the specific choice of  $L_1$ , while  $d\Gamma$  the result of a change in the angle of attack, or a local modification of the TE geometry).

Although the relation between lift and circulation (Kutta-Joukovsky) is in general valid only for potential incompressible flow, the concept of circulation as proxy for the lift also under the current compressible flow conditions is used with the particular objective

**Table 5** Circulation

Configuration	Clean	Straight 2% <i>c</i>
$\Gamma_1/(V_\infty \cdot c)$ (Ma=0.70, $\alpha=3.5^\circ$ )	1.07	1.08
$\Gamma_1/(V_\infty \cdot c)$ (Ma=0.74, $\alpha=2.5^\circ$ )	1.04	1.08

**Fig. 17** Circulation value ( $\Gamma_1/(V_\infty \cdot c)$ ) per buffet phase



to assess if the measured flow fields allow to infer whether the UTEF affects circulation, hence, the (mean) lift value. This choice is substantiated by the study of Liu et al. (2015), which shows that in the low transonic Mach numbers regime (as in this study) the classical lift equation derived by Joukowski can be applied to evaluate the lift coefficient obtaining a good estimation of the lift coefficient also for a circulation contour passing in proximity of the trailing edge of the airfoil.

In this study  $\Gamma_1$  has been evaluated sufficiently far from the surface of the airfoil and from the trailing edge (see Fig. 10), and results in a value of  $\Gamma_1/(V_\infty \cdot c)=1.08$  for the straight 2% UTEF and 1.07 for the clean configuration (see Table 5). This estimation shows that the use of a UTEF does not significantly reduce the value of the circulation, which is actually slightly increased (although this difference is of the same order of the uncertainty in the evaluation of the circulation).

As similar values of  $\Gamma_1$  are found along  $L_1$ , with and without the straight UTEF, this justifies the assumption of considering  $\Gamma_0$  constant and thus, can reasonably conclude that also the total circulation  $\Gamma$  is not appreciably changed by the UTEF under the current conditions. This observation brings to the conclusion that the use of a UTEF is expected to mitigate buffet, not affecting the operative flight condition (same Ma and approximately same lift coefficient).

In addition, this analysis has been repeated for the phase averaged velocity fields, for both the clean and the straight UTEF configurations and the results plotted in Fig. 17.

The plot shows that the values of circulation are distributed almost sinusoidally along the different buffet phases. In presence of UTEFs not only does the average value of  $\Gamma_1/(V_\infty \cdot c)$  slightly increase (by about 1%) but also the amplitude of oscillation of  $\Gamma_1/(V_\infty \cdot c)$  during the buffet cycle is reduced by nearly 50% when compared to the clean airfoil. Under the assumption that the variation of  $\Gamma_0$  with phase is the same for both configurations, this

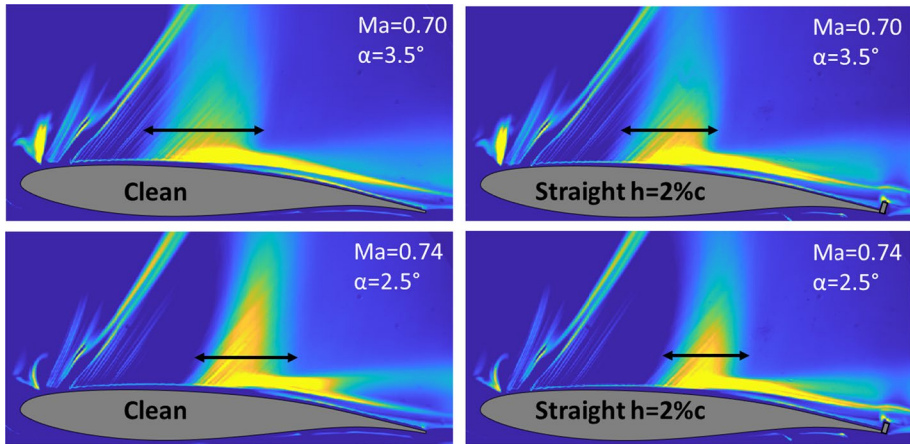


**Fig. 18** Standard deviation of schlieren images for  $Ma=0.70, \alpha=3.5^\circ$  and  $Ma=0.74, \alpha=2.5^\circ$ . The arrows indicate the shockwave oscillation ranges

**Table 6** Shock positions statistics

Configuration	$(X_{SW})_{avg} (\%c)$	$(X_{SW})_{std} (\%c)$
Clean, $Ma=0.70, \alpha=3.5^\circ$	40	7
Clean, $Ma=0.74, \alpha=2.5^\circ$	48	4
Straight 2%c, $Ma=0.70, \alpha=3.5^\circ$	41	5
Straight 2%c, $Ma=0.74, \alpha=2.5^\circ$	50	4

result further suggests that in presence of UTEFs, the oscillation of the aerodynamic loads is diminished as well.

### 5 Sensitivity of UTEF Operation to the Flow Condition

To show the sensitivity of the UTEF to the specific flow condition, the behavior of both the clean and the straight UTEF 2% configuration is investigated for an additional flow condition:  $Ma=0.74$  and  $\alpha=2.5^\circ$  (a condition where buffet is less developed). In order to provide a comparison of the relevance of the shock oscillations for both the flow conditions and configurations, the standard deviation of the intensity of luminosity of the schlieren images is shown in Fig. 18. The first thing that stands out in the plots is the reduced spatial range of the shock wave oscillation at  $Ma=0.74, \alpha=2.5^\circ$  compared to  $Ma=0.70, \alpha=3.5^\circ$ , for both the UTEF and the clean cases. In addition, the average shock wave position is located more downstream for  $Ma=0.74, \alpha=2.5^\circ$ , as expected. This data is summarized in Table 6, which confirms that the fluctuations of the shock wave position are reduced for  $Ma=0.74, \alpha=2.5^\circ$ .

When comparing the clean configuration with the 2% straight UTEF for  $Ma=0.74, \alpha=2.5^\circ$  (Fig. 18, bottom), the range of oscillation appears very similar with a slight reduction of the shock wave oscillation area in presence of the UTEF. An upwash is again visible at the trailing edge when the UTEF is used, together with higher fluctuations in the shear

layer. These observations suggest that the UTEF has still a beneficial effect in reducing the separated region.

An evaluation of the  $\Gamma_1$  term of the circulation from the PIV data shows that, also for this flow condition, there is a slight increase of circulation in presence of UTEF (as reported in Table 5).

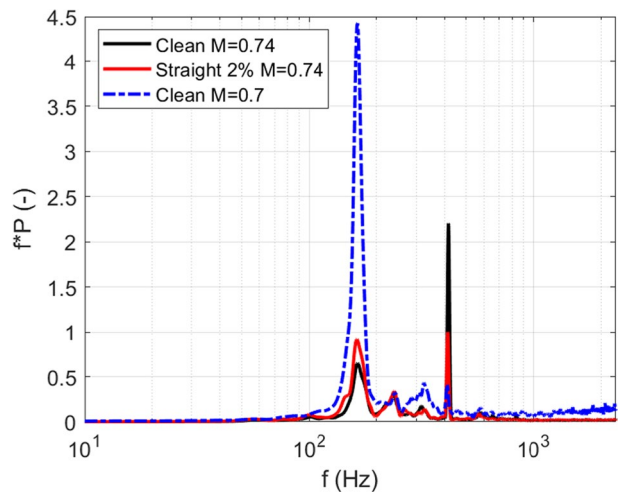
The spectral content of the shock position is once again evaluated by means of a PSD (see Fig. 19) and the values compared to the PSD of the clean configuration at  $Ma=0.70$ ,  $\alpha=3.5^\circ$  (dashed line). There is a sharp reduction of the peak at the main buffet frequency of 160 Hz, when moving to the off-buffet condition, both for the UTEF and the clean case. On the other hand, with the increase of the Mach number, an increase of a peak at 410 Hz is observable (although this peak is reduced by more than 50% in presence of the straight UTEF). As previously mentioned this peak is associated with wind tunnel noise, which becomes more important at a higher Mach number. A similar contribution of the buffet peak (at 160 Hz) is observed for the two configurations tested at  $Ma=0.74$  (slightly lower for the clean case), in agreement with the values of  $(X_{SW})_{std}$  (see Table 6). These results show that buffet unsteadiness is not increased for this secondary flow condition, however, to experimentally exclude that the use of a UTEF does not simply shift the occurrence of the most developed buffet condition, additional tests at other values of  $Ma$  and  $\alpha$  are required.

## 6 Conclusion

In this study the use of trailing edge flaps with an upward deflection (UTEFs), demonstrated to be effective in controlling transonic buffet, in particular when using a straight 2% UTEF.

The results show that buffet is not completely suppressed, but significantly reduced in intensity. Both the shock wave and separated area are characterized by a reduced amplitude of oscillation in the UTEF case, although always with a main frequency contribution at 160 Hz (see Fig. 9, left and Fig. 14, right). In addition to the reduced pulsation of the separated area in presence of a straight UTEF, the separated area is also characterized by

**Fig. 19** PSD of shock wave position for  $Ma=0.74$ ,  $\alpha=2.5^\circ$  for clean and straight 2% configurations





a reduction of its extent (see Table 4), having important consequence in alleviating shock buffet.

Although an estimation of the drag coefficient was out of the scope of this work, using as a proxy the size of the separated area, it is speculated that for the straight UTEF configuration, the drag coefficient would be reduced as well.

The behavior of the shock wave position appears more irregular in presence of the straight 2%*c* UTEF configuration compared to the smoother behavior for the clean airfoil (see Fig. 7) and a similar behavior is present for the separated area. These results confirm that with the use of the UTEF the coherence of the buffet oscillation can be considered to be interrupted, as also shown in Fig. 15, where the correlation between the shock wave position and the separated area extent weakens for the straight UTEF compared to the clean airfoil.

The analysis of the data for the serrated UTEFs has assisted the understanding of the performance of the straight UTEFs. As shown in Sect. 4.3 the presence of a serrated UTEF has a non-negligible effect on the mean flow, with a different behavior in the planes corresponding to the peak or the valley of the serration. Nonetheless, no significant variation is observed in terms of the overall transonic buffet properties, confirming the inefficacy of a serration in compressible flows, in agreement with Nies and Oliver (2013).

When straight UTEFs are used, the direct communication between the suction side of the airfoil and the trailing edge is inhibited. As a consequence fewer (or weaker) UTWs are generated resulting in a reduction of the shock oscillation range. The hesitation of the shock position could be associated with the fact that the UTWs are still reaching the shock wave but in a more intermittent fashion (at least in strength). On the other hand, when a serrated UTEF is used, the communication between the vortical structures in the separated area (DTWs) and the trailing edge itself remains present, particularly in correspondence to the valley of the serration. Since the UTWs are pressure waves that travel upstream in a quasi-hemispherical way, the UTWs created in the valley area of a serration do not only communicate with the shock wave at that specific span location, but along a spanwise extended area. This suggests that the UTEFs are effective in reducing buffet properties only when the connection between the separated area and the trailing edge is inhibited along the full span, as in the case for a straight UTEF. The possible effect of the straight UTEFs on the production of the UTWs at the trailing edge, and the consequent reduction of the shock wave oscillations, supports the feedback mechanism description of transonic buffet.

The performance of UTEFs of different heights has shown that a relevant reduction of the shock oscillation properties is obtained only when the height of the UTEF is equal or higher than the height of boundary layer near the trailing edge of the airfoil, as clear from the results shown in Fig. 9 (right). This evidence suggests that the vortices which are responsible for the production of UTWs are traveling downstream very close to the surface of the airfoil in agreement with what proposed by D'Aguzzo et al. (2021c).

The use of UTEFs clearly modifies the geometry of the airfoil, so it could be conceived that the observed buffet reduction is the result of a change of the airfoil operating condition, which shifts the most developed buffet condition to higher Mach numbers or angles of attack, because of a possible change in circulation around the airfoil. However, estimates obtained from the PIV data showed that the average circulation value is not affected appreciably by the introduction of UTEFs while its oscillation range is reduced by nearly 50%.

These results confirm findings obtained in the numerical study of Tian et al. (2018), where an increase of the buffet onset for both the angle of attack and the lift coefficient was achieved when using similar devices. The performance of the UTEF has also been checked for a less developed buffet condition, corresponding to a Mach number of 0.74

and  $\alpha = 2.5^\circ$ . The results showed that even under this condition the use of a straight 2% UTEF proved beneficial, achieving a slight reduction of the shock buffet oscillation range (see Fig. 18) with respect to the clean configuration and a slight increase of the circulation value. Thus, differently from other passive systems used for the control of transonic buffet, UTEFs demonstrated to be more versatile in reducing the unsteadiness connected with buffet and their efficacy proved not to be strongly dependent on the specific buffet condition, since their working principle is associated with the disruption of the communication between DTWs and UTWs in the feedback cycle rather than of a change (reduction) of the circulation, as opposed to the working mechanism of more conventional TEDs.

In practice, to optimize buffet control performance whilst avoiding any undesired effect in other (i.e. non-buffet) flow conditions, one could imagine to apply UTEFs to future aircraft in the form of deployable devices, or by means of folding trailing edges, to be activated only under (potential) buffet conditions.

**Author Contribution** All authors contributed to the study conception, design and preparation. Data collection and analysis were performed by AD'A. The first draft of the manuscript was written by AD'A and all authors commented on previous versions of the manuscript. All authors read and approved the final manuscript.

**Funding** This work has been carried out as part of the project HOMER (Holistic Optical Metrology for Aero-Elastic Research), funded by the European Commission, program H2020 under Grant No. 769237.

## Declarations

**Conflict of Interest** The authors declare they have no conflict of interest.

**Ethical Approval** Not applicable.

**Informed Consent** All authors have been informed and gave explicit consent to submit the paper.

**Open Access** This article is licensed under a Creative Commons Attribution 4.0 International License, which permits use, sharing, adaptation, distribution and reproduction in any medium or format, as long as you give appropriate credit to the original author(s) and the source, provide a link to the Creative Commons licence, and indicate if changes were made. The images or other third party material in this article are included in the article's Creative Commons licence, unless indicated otherwise in a credit line to the material. If material is not included in the article's Creative Commons licence and your intended use is not permitted by statutory regulation or exceeds the permitted use, you will need to obtain permission directly from the copyright holder. To view a copy of this licence, visit <http://creativecommons.org/licenses/by/4.0/>.

## References

- Babinsky, H., Harvey, J.: Shock wave-boundary-layer interactions, Cambridge aerospace series. Cambridge University Press (2011)
- Brion, V., Dandois, J., Mayer, R., Reijasse, P., Lutz, T., Jacquin, L.: Laminar buffet and flow control. Proc. Inst. Mech. Eng. Part G J. Aerosp. Eng. **234**(1), 124–139 (2019). <https://doi.org/10.1177/0954410018824516>
- Bruce, P.J.K., Colliss, S.P.: Review of research into shock control bumps. Shock Waves **25**(5), 451–471 (2015). <https://doi.org/10.1007/s00193-014-0533-4>
- Brutyan, M., Volkov, A., Potapchik, A.: An experimental study of a passive method of attenuating a transonic buffet phenomenon. Tech. Phys. Lett. **45**, 1082–1084 (2019). <https://doi.org/10.1134/S106378501911004X>

- Caruana, D., Mignosi, A., Robitaille, C., Corrège, M.: Separated flow and buffeting control. *Flow Turbul. Combust.* **71**(1), 221–245 (2003). <https://doi.org/10.1023/B:APPL.0000014918.93432.4f>
- Caruana, D., Mignosi, A., Corrège, M., Le Pourhiet, A., Rodde, A.M.: Buffet and buffeting control in transonic flow. *Aerosp. Sci. Technol.* **9**(7), 605–616 (2005). <https://doi.org/10.1016/j.ast.2004.12.005>
- Colliss, S.P., Babinsky, H., Nübler, K., Lutz, T.: Vortical structures on three-dimensional shock control bumps. *AIAA J.* **54**, 2338–2350 (2016). <https://doi.org/10.2514/1.J054669>
- Crouch, J.D., Garbaruk, A., Magidov, D.: Predicting the onset of flow unsteadiness based on global instability. *J. Comput. Phys.* **224**(2), 924–940 (2007). <https://doi.org/10.1016/j.jcp.2006.10.035>
- D'Aguanno, A., Schrijer, F.F.J., van Oudheusden, B.W.: Spanwise organization of upstream traveling waves in transonic buffet. *Phys. Fluids* **33**(10), 106105 (2021a). <https://doi.org/10.1063/5.0062729>
- D'Aguanno, A., Schrijer, F.F.J., van Oudheusden, B.W.: Experimental investigation of the transonic buffet cycle on a supercritical airfoil. *Exp. Fluids* **62**, 214 (2021c). <https://doi.org/10.1007/s00348-010-0892-2>
- D'Aguanno, A., Schrijer, F.F.J., van Oudheusden, B.W.: Investigation of 3D shock control bumps for transonic buffet alleviation. In: *AIAA 2021b-2558, AIAA Aviation (2021b) Forum*, 02–06 August (2021b). <https://doi.org/10.2514/6.2021-2558>
- de Kat, R., van Oudheusden, B.W.: Instantaneous planar pressure determination from PIV in turbulent flow. *Exp. Fluids* **52**(5), 1089–1106 (2012). <https://doi.org/10.1007/s00348-011-1237-5>
- Deck, S.: Numerical simulation of transonic buffet over a supercritical airfoil. *AIAA J.* **43**(7), 1556–1566 (2005). <https://doi.org/10.2514/1.9885>
- Despre, C., Caruana, D., Mignosi, A., Reberga, O., Corrège, M.: Buffet active control - experimental and numerical results. In: *proceedings of RTO AVT symposium on active control technology of enhanced performance operational capabilities of military aircraft, land vehicles, and sea vehicles*, June, Germany (2001).
- Feldhusen-Hoffmann, A., Lagemann, C., Loosen, S., Meysonnat, P., Klaas, M., Schröder, W.: Analysis of transonic buffet using dynamic mode decomposition. *Exp. Fluids* **62**(4), 66 (2021). <https://doi.org/10.1007/s00348-020-03111-5>
- Gao, C., Zhang, W., Ye, K.: Numerical study on closed-loop control of transonic buffet suppression by trailing edge flap. *Comput. Fluids* **132**, 32–45 (2016). <https://doi.org/10.1016/j.compfluid.2016.03.031>
- Garnier, E., Deck, S.: Large-eddy simulation of transonic buffet over a supercritical airfoil. In: *Armenio, V., Geurts, B., Fröhlich, J. (eds.) Direct and large-eddy simulation VII*, pp. 549–554. Springer, Dordrecht (2010). [https://doi.org/10.1007/978-90-481-3652-0\\_81](https://doi.org/10.1007/978-90-481-3652-0_81)
- Geoghegan, J.A., Giannelis, N.F., Vio, G.A.: A numerical investigation of the geometric parametrisation of shock control bumps for transonic shock oscillation control. *Fluids* **5**(2), 46 (2020). <https://doi.org/10.3390/fluids5020046>
- Giannelis, N.F., Vio, G.A., Levinski, O.: A review of recent developments in the understanding of transonic shock buffet. *Prog. Aerosp. Sci.* **92**, 39–84 (2017). <https://doi.org/10.1016/j.paerosci.2017.05.004>
- Hartmann, A., Feldhusen, A., Schröder, W.: On the interaction of shock waves and sound waves in transonic buffet flow. *Phys. Fluids* **25**(2), 026101 (2013). <https://doi.org/10.1063/1.4791603>
- Herriot, J.G.: Blockage corrections for three dimensional flow closed throat wind tunnels, with consideration of the effect of compressibility. In: *NACA Report No. 995* (1950).
- Hilton, W.F., Fowler, R.G.: Photographs of shock wave movement. Technical Report No. 2692, HM Stationery Office (1952).
- Humble, R.A.: Unsteady flow organization of a shock wave/boundary layer interaction. In: *PhD thesis, Delft University of Technology*, ISBN: 978-90-597-2295-8 (2009).
- Jacquín, L., Molton, P., Deck, S., Maury, B., Soulevant, D.: Experimental study of shock oscillation over a transonic supercritical profile. *AIAA J.* **47**(9), 1985–1994 (2009). <https://doi.org/10.2514/1.30190>
- Lee, B.H.K.: Transonic buffet on a supercritical aerofoil. *Aeronaut. J.* **94**, 143–152 (1990). <https://doi.org/10.1017/S0001924000022752>
- Lee, B.H.K.: Effects of trailing-edge flap on buffet characteristics of a supercritical airfoil. *J. Aircr.* **29**(1), 93–100 (1992). <https://doi.org/10.2514/3.46130>
- Liu, L., Zhu, J., Wu, J.: Lift and drag in two-dimensional steady viscous and compressible flow. *J. Fluid Mech.* **784**, 304–341 (2015). <https://doi.org/10.1017/jfm.2015.584>
- Mayer, R., Lutz, T., Krämer, E.: Numerical study on the ability of shock control bumps for buffet control. *AIAA J.* **56**(5), 1978–1987 (2018). <https://doi.org/10.2514/1.J056737>
- Molton, P., Dandois, J., Lepage, A., Brunet, V., Bur, R.: Control of buffet phenomenon on a transonic swept wing. *AIAA J.* **51**, 761–772 (2013). <https://doi.org/10.2514/1.J051000>
- Nies, J.M., Olivier, H.: Dependence of upstream moving pressure waves on the Mach number and the impact of trailing edge serrations. In: *62. Deutscher Luft- und Raumfahrtkongress*, 10–12 Sept, Stuttgart (2013).

- Ogawa, H., Babinsky, H., Pätzold, M., Lutz, T.: Shock-wave/boundary-layer interaction control using three-dimensional bumps for transonic wings. *AIAA J.* **46**(6), 1442–1452 (2008). <https://doi.org/10.2514/1.32049>
- Ragni, D., Schrijer, F.F.J., van Oudheusden, B.W., Scarano, F.: Particle tracer response across shocks measured by PIV. *Exp. Fluids* **50**(1), 53–64 (2011). <https://doi.org/10.1007/s00348-010-0892-2>
- Ren, K., Chen, Y., Gao, C., Zhang, W.: Adaptive control of transonic buffet flows over an airfoil. *Phys. Fluids* **32**, 096106 (2020). <https://doi.org/10.1063/5.0020496>
- Sartor, F., Minervino, M., Wild, J., Wallin, S., Maseland, H., Dandois, J., Soudakov, V., Vrchota, P.: A CFD benchmark of active flow control for buffet prevention. *CEAS Aeronaut. J.* **11**, 837–847 (2019). <https://doi.org/10.1007/s13272-019-00415-z>
- Schrijer, F.F.J., Scarano, F.: Effect of predictor-corrector filtering on the stability and spatial resolution of iterative PIV interrogation. *Exp. Fluids* **45**(5), 927–941 (2008). <https://doi.org/10.1007/s00348-008-0511-7>
- Suresh, M., Sitaram, N.: gurney flap applications for aerodynamic flow control. In: Proceedings of the 9th International Conference on Mechanical Engineering, 18–20 December, Dhaka (2011).
- Tian, Y., Li, Z., Liu, P.Q.: Upper trailing-edge flap for transonic buffet control. *J. Aircr.* **55**(1), 382–389 (2018). <https://doi.org/10.2514/1.c033134>
- Wanga, J., Lia, Y., Choi, K.: Gurney flap -lift enhancement, mechanisms and applications. *Prog. Aerosp. Sci.* **35**(12), 1890–1891 (2008)
- Welch, P.: The use of fast Fourier transform for the estimation of power spectra: a method based on time averaging over short, modified periodograms. *IEEE Trans. Audio Electroacoust.* **15**, 70–73 (1967)
- Westerweel, J., Scarano, F.: Universal outlier detection for piv data. *Exp. Fluids* **39**, 1096–1100 (2005). <https://doi.org/10.1007/s00348-005-0016-6>
- Zhang, Y., Yang, P., Li, R., Chen, H.: Unsteady simulation of transonic buffet of a supercritical airfoil with shock control bump. *Aerospace* **8**(8), 203 (2021). <https://doi.org/10.3390/aerospace8080203>

**Publisher's Note** Springer Nature remains neutral with regard to jurisdictional claims in published maps and institutional affiliations.